Title:

Xenon-induced inhibition of synchronized bursts in a rat cortical neuronal network

Authors' names and affiliations:

T. Uchida [a*], S. Suzuki [a], Y. Hirano [a], D. Ito [a], M. Nagayama [a], K. Gohara [a]

[a] Division of Applied Physics, Faculty of Engineering, Hokkaido University, N13 W8 Kita-ku, Sapporo 060-8628, Japan

*Corresponding author

Postal address: Division of Applied Physics, Faculty of Engineering, Hokkaido University, N13 W8 Kita-ku, Sapporo 060-8628, Japan

Tel & fax: +81-11-706-6635

E-mail address: t-uchida@eng.hokudai.ac.jp (TU)

List of abbreviations:

Xe, xenon; DIV, day *in vitro*; DMEM, Dulbecco's Modified Eagle Medium; MEA, multi-electrode array; MED, multi-electrode dish; $GABA_A$, γ-aminobutyric acid type-A; NMDA, N-methyl-D-aspartate; SR, spike rate; SBR, synchronized-burst rate; SA, spike amplitude; SW, spike width; BD, burst duration; IBI, inter-burst interval, SIB, number of spikes in a burst

Abstract:

Xenon (Xe) and other inert gases produce anesthesia via an inhibitory mechanism in neuronal networks. To better understand this mechanism, we measured the electrical signals from cultured rat cortical neuronal networks in a multi-electrode array (MEA) under an applied Xe pressure. We used the MEA to measure the firing of the neuronal network with and without Xe gas pressurized to 0.3 MPa. The MEA system monitored neuronal spikes on 16 electrodes (each 50×50 μm^2) at a sampling rate of 20 kHz. The embryo rat cortical cells were first cultured on MEAs without Xe for approximately three weeks, at which time they produced synchronized bursts that indicate maturity. Then, with an applied Xe pressure, the synchronized bursts quickly ceased, whereas single spikes continued. The Xe-induced inhibition-recovery of neuronal network firing was reversible: after purging the Xe from the system, the synchronized bursts gradually resumed. Thus, Xe did not inhibit single neuron firing, yet reversibly inhibited the synaptic transmission. This finding agrees with the channel-blocker and a modified-hydrate hypothesis of anesthesia, but not the lipid-solubility hypothesis. (174 words)

Keywords:

General anesthesia; multi-electrode array; synapse transmission inhibition; xenon molecule

INTRODUCTION

General anesthesia is thought to be caused by the inhibition of neuronal firing from an agonist and/or an antagonist. One anesthetic is xenon (Xe), an inert gas that produce general anesthesia without causing undesirable side effects [Cullen and Gross, 1951]. But the Xe-anesthesia mechanism remains unclear.

The Xe anesthetic effect was first thought to be caused by the cell membrane swelling with Xe [Miller et al., 1965; Miller, 1969; Lever et al., 1971; Koski et al., 1973; O'leary, 1984] due to Xe's high solubility in lipids [Meyer, 1937]. On the other hand, Pauling [1961] and Miller [1961] proposed the hydrate hypothesis in which the signals are inhibited by a clathrate hydrate at synapses. Although this hypothesis was opposed by several researchers [e.g.,Miller, 1969], it has received support from theoretical [Dorsch, 1970; Dorsch and deRocco, 1973], experimental [Schoenborn et al., 1964; Dorsch and Distefano, 1973] and clinical [Matsumoto, 1995] investigations. Recently, several pharmacological studies suggest that Xe molecules act as the antagonist of glutamate–induced channels. This mechanism differs from that of other general anesthetic agents, such as isoflurane and halothane, which activate the inhibitory γ-aminobutyric acid type-A ($GABA_A$) receptor channels [Franks and Lieb, 1982; 1988; 1994; Mihic et al., 1997]. Some researchers claimed that Xe molecules strongly inhibit the excitatory N-methyl-D-aspartate (NMDA) receptor channels [Franks et al., 1998; de Sousa et al., 2000; Ma et al., 2002; Nagale et al., 2005], but others suggested the target to be non-NMDA receptor channels [Plested et al., 2004] or both [Dinse et al., 2005; Preckel et al., 2006; Haseneder et al., 2008; Georgiev et al., 2010]. Therefore, several general anesthetic mechanisms of Xe gas are under consideration.

The functioning of neurons in culture samples has made possible various studies in the field of neuroscience. When dissociated neurons start contacting each other via synapse formation, neuronal cells and networks show primitive patterns of synchronized activity by groups of

neurons. Such patterns of electric activity occur in an early phase of network formation, often in close similarity to those seen *in vivo* [Ben-Ari, 2001; Corner et al., 2002; Khazipov et al., 2004]. The pioneering work of Gross [1979], Gross and Schwalm [1994] and of Pine [1980] has evolved to the point where, as later shown by Robinson et al. [1993] and Jimbo et al. [1999], long-term multi-electrode registration can be used to study activity-dependent plasticity at the synaptic level. Dissociated neurons cultured *in vitro* autonomously form complicated networks that spontaneously show synchronized bursts [Kamioka et al., 1996; Opitz et al., 2002; Ito et al., 2010] that are highly variable in terms of their spatio-temporal firing patterns, yet highly correlated among neurons [van Pelt et al., 2004; Chiappalone et al., 2006; Wagenaar et al., 2006]. Therefore, neuronal cultures *in vitro* on multi-electrode arrays (MEAs) are a useful tool for modeling the maturation of the neuronal networks and their electrophysiological properties.

We developed a model system for rat cortical neuronal networks *in vitro* on MEAs [Ito et al., 2010] to measure the development of neuronal electric activity. This system is useful to understand the spatiotemporal single spikes and bursts, not only for single neurons but also for the neuronal network. Here we apply this system to the Xe-anesthesia problem by exposing the neuronal network to pressurized Xe gas. We find that the pressurized Xe gas inhibits the synchronized bursts, but leaves the single spikes essentially unchanged.

EXPERIMENTAL PROCEDURES

Cell culture on MEAs

The sample preparation was almost the same as that in our previous work [Ito et al., 2010], so here we give only a brief description. Dissected cortex was prepared from Wistar rats at embryonic day 17 using the Nerve-Cell Culture System (Sumitomo Bakelite, Tokyo, Japan) as

described previously [Mizuno et al., 2004; Banno et al., 2005; Takeuchi et al., 2005]. Cortices were dissociated into single cells using dissociation solution (mainly papain), and then resuspended in Neuron Culture Medium (Sumitomo Bakelite; serum-free conditioned medium from 48-h rat astrocyte confluent cultures based on Dulbecco's modified Eagle's minimum essential medium (DMEM)/F-12 with N2 supplement, [Banno et al., 2005; Takeuchi et al., 2005]). Dissociated neuron was plated with a nominal density of 2500 cells/mm^2 onto a poly(ethylenimine)-coated multi-electrode dish (MED) probe (Alpha MED Scientific, Osaka, Japan). The probe consisted of 64 planar microelectrodes and 4 reference electrodes [Kudoh et al., 2007; Hosokawa et al., 2008; Ito et al., 2010]. Each electrode was 50×50 μm^2 and the electrode spacing was 150 μm. To avoid cell attachment onto reference electrodes, we used a cloning ring with an inner diameter of 5 mm and total area of 19.6 mm^2 [Homma et al., 1998]. The rings were removed after adhesion of neurons on the MED probe (approximately 3h).

The cultures were incubated in the neuron culture medium in a humidified atmosphere containing 5% CO_2 and 95% air at 37°C (that is, the physiological condition). After 3 days in the neuron culture medium (twice a week), half of the medium was replaced with fresh DMEM/serum medium, which consisted of DMEM (Invitrogen-Gibco, Carlsbed, CA, USA) supplemented with 5% fatal bovine serum (Invitrogen-Gibco), 5% horse serum (Sigma-Aldrich, St. Louis, MO, USA), 25 μg/mL insulin (Invitrogen-Gibco), 100 U/mL penicillin, and 100 μg/mL streptomycin (Invitrogen-Gibco) [Ito et al., 2010]. Thus the Neuron Culture Medium is gradually replaced to the DMEM/serum medium during culture. The adhesion, growth, and morphological changes of cultured neurons were observed under a phase-contrast microscope (Olympus, Tokyo, Japan; type CKX-41).

Firing-activity measuring system

The firing activity of each cortical culture was recorded at a sampling rate of 20 kHz using a

MED64 extracellular recording system (Alpha MED Scientific), and the A/D conversion was done with the MED64 conductor software. To observe the neuronal network maturation, we measured the firing activities of cultured neurons on the MED probe several times per week. Based on the firing activity exhibiting periodical synchronized bursts, the samples used in the gas-pressurizing experiments were between 20 and 30 days *in vitro* (DIV).

To measure the firing activities under pressurized gas conditions, we constructed a high-pressure vessel equipped with the MED connector (Taiatsu Techno, Tokyo, Japan). Since the measurement system was in a non-humidified incubator, the MED probes of cortical cultures were taken from the cultivation incubator. The pressure was monitored by a pressure transducer (Yokogawa; type FP201-C22-C20A*B) and the pressure could reach 1 MPa. The cell shape was monitored through the pressure-proof glass windows by a macro-zoom lens + CCD camera system (Elmo, Nagoya, Japan; type TVZ610M-P). The 16 electrodes at the center of the MED probe could be monitored in this vessel. The system was placed in an incubator (Fukushima Industry, Osaka, Japan; type FMU-132I) in which the temperature was controlled within ±1°C. A type-T thermocouple measured the temperature in the vessel. Pressure and temperature were recorded by a data logger (Graphtec, Yokohama, Japan; type GL400). The whole system is illustrated in Fig. 1.

The experimental procedure has four periods, distinguished by the gas pressure and gas composition. Traces are shown in Fig. 2 and described as follows. Period (I), the control period: After reducing the culture medium to less than half of its original volume (to minimize the time-lag due to the dissolution process of gas in the medium), the MED probe with the cortical culture was put in the high-pressure vessel and incubated at 38.5 ±1°C while the firing activity was measured. Period (II), the pressurizing period: Following the control period, Xe gas was introduced to the vessel at a gauge pressure of approximately 0.3 MPa. Because the original atmospheric air had a pressure of 0.1 MPa, the Xe fraction in the gas of the vessel is 0.75 and the total ambient pressure is 0.4 MPa. We applied Xe gas at this pressure because a

Xe concentration of 75% in the vessel approximates the minimal Xe concentration effective for human anesthesia of about 71% [Goto et al., 1997]. The pressurizing period lasted one hour. Period (III), the pressure-released period: The release valve was opened to reduce the pressure in the vessel to atmospheric pressure (0.1 MPa). However, the gas composition in the vessel is still Xe-rich. Period (IV), the purge period: One hour after the depressurization, we let the purging gas flow for several minutes to flush out the Xe in the vessel. After 1-h of measurements in this period, we returned the MED probe to the cultivation incubator. Then, several days after the experiment, we checked the cultured sample for damages. To check the reproducibility of the results, we ran the experiments for eight different cultured samples.

The Xe gas used for in experiments had purity 99.995% (Air-Water, Wakayama, Japan) and the purging gas was air that contained 5% CO_2 (Hokkaido Air-Water, Sapporo, Japan). The purging gas had the same composition as that in the cultivation incubator.

Characterization of spikes and bursts

The detection procedures and criteria for spikes and synchronized bursts are the same as those in Ito et al., [2010]. A spike was identified when the intensity of the extracellular potential exceeded a threshold within a window of 1ms (Fig. 3a). To determine the threshold, we evaluated the level of biological and thermal noises (usually 10~20 μV) over the complete data set for the experiment and then applied the tangent-method described in Ito et al. [2010]. For all 16 electrodes (area of 650×650 μm^2 in a MED probe), we plotted the single spikes and synchronized bursts in a spike raster-plot, and then counted the spike rate (*SR*) and synchronized-burst rate (*SBR*) over all 16 electrodes. A burst is defined here as a time period with spike density exceeding 2 per 100 ms [Ito et al., 2010]. Bursts were detected using the method described in Mukai et al. [2003].

To evaluate the profile change of single spikes and bursts before, during, and after Xe

pressurization, we characterized the profiles of single spikes and bursts on a typical electrode by five parameters. Single spikes were characterized by their spike amplitude (*SA*) and spike width (*SW*) as shown in Fig. 3a. (Although the field potential observed on one electrode was the total firing activities of all neurons located near the electrode, qualitative comparisons of the profiles nevertheless indicate average changes in neuronal activity.) Burst profiles are highly variable [Wagennar et al., 2006], but can be characterized by three parameters: the burst duration (*BD*), the inter-burst interval (*IBI*) and the number of spikes in a burst (*SIB*), all of which are sketched in Fig. 3b. *IBI* was determined as the time difference between the last spike of one burst and the first spike of the subsequent burst.

RESULTS

Period (I): Control period electric activity

In the early stage of the cultivation, the dispersed rat cortical neurons adhered to and spread out on both the glass plate and electrodes on the MED probe (Fig. 4a left). The neurons gradually contacted each other to form a network and started firing about 1 week after the cultivation began. *SR* increased with time (Fig. 4b), and both neurons and glial cells grew to reach the confluent condition at approximately 2 weeks (Fig. 4a right). At this time, *SR* stopped increasing on average, and thereafter stayed in the range of $4\sim8\times10^3$ counts/min (Fig. 4b). This is consistent with our previous work [Ito et al., 2010]. The confluent condition also brought frequent synchronized bursts (Fig. 5a). The spike raster plot (Fig. 5b) indicates that most spikes were within synchronized bursts, with a few single spikes observed between the bursts in the limited number of electrodes.

Roughly steady-state behavior began after about 2 weeks in culture. Figs. 4b and 5b show that all 16 electrodes were active with *SR* averaging approximately 5×10^3 counts/min. (Note that the absolute value of *SR* varied with the sample). The average profile of single spikes between bursts in the control period was almost constant, with $SA \approx 25$ μV and $SW \approx 1$ ms.

The bursts were more variable, with *SBR* ranging between 10 and 30 counts/min, *BD* on the typical electrode averaging approximately 0.25 s with a standard deviation of 0.2 s (Fig. 7b), and *IBI* varying mainly between 1 and 15 s (Fig. 7c). *SIB* gradually ranges between 30 and 60 counts per burst (cpb) (Fig. 7d).

Period (II): Synchronized bust inhibition under Xe pressurization

Although the optical microscope revealed no morphological change after applying the Xe pressure, the firing activities of the neuronal network drastically changed. As shown in Figs. 6a and b, the synchronized bursts gradually decreased and, after approximately 10 min, finally disappear, which indicates that pressurized Xe gas inhibits synchronized bursts. However, single spikes still occurred on more than 60% of firing electrodes (Figs. 6c and d). Moreover, some bursts still occurred in few electrodes (e.g., electrodes #3 and #9 in Fig. 6d). About 10% of the electrodes in each experiment produced a series of frequent single spikes during the Xe- pressurization (e.g., #4 and #28 in Fig. 6d) even though they had a lower *SR* in the control period. Thus, the data indicates that Xe gas does not completely inhibit the firing activity.

The sudden decrease of *SR* after pressurization results from the simultaneous disappearance of synchronized bursts (Fig. 7a) although the non-burst single-spike rate does not change remarkably. After decreasing, *SR* remains remarkable constant at approximately 1×10^3 counts/min. These single spikes and a small number of local bursts occurred throughout the Xe-pressurization period. Concerning the spike profile, the averaged profile of the single spike was almost the same as that in the control period, that is, *SA* and *SW* were 25 μV and 1 ms, respectively. These results suggest that the Xe pressurization inhibits only the synchronized bursts of the neuronal network.

During the transition between periods I and II, some burst parameters changed, but not right away (Figs. 7b-d). Within the first 5 min of pressurization, the profile parameters show little

change. This result suggests that the change of hydrostatic pressure affected neither the firing pattern of the neuronal network nor the single spikes. However, approximately 5-min after the pressurization, *IBI* increases while maintaining a fluctuation range similar to that in the control period. Then 10-min after pressurization, *IBI* effectively reaches infinity, making the disappearance of the synchronized bursts. Also, as *BD* shows a slight decrease with *SIB*, the firing frequency for burst decreases as *SBR* decreases.

Period (III): Recovery of electric activity with pressure release

As with the previous transition (I-II), the microscope observation revealed no morphological change when the pressurized Xe gas was released. Moreover, despite the estimated Xe concentration of approximately 0.14 mol/mL in the medium during period (II), the depressurization process in (III) did not produce observable bubbles. This result means that the release of dissolved Xe molecules from aqueous solution was too slow for bubble formation. This slow release is consistent with the observed slow recovery of the firing activity.

The synchronized bursts did not start to return until about 10~30 min after the pressure release. Then, although the non-burst single-spike rate does not change, both *SR* and *SBR* increase gradually with time throughout the period (Figs. 8 and 9a). This increase arose mainly from the decrease of *IBI* to ~1 s. Compared to those in the control period, the bursts had slightly larger *BD* values, through with wide scatter (up to 1 s) and smaller *SIB* value (approximately 20 cpb). *SBR* continues to increase throughout the period and both *BD* and *SIR* may have recovered to the original variation range. The recovery of firing activity was very slow compared to the inhibition in period (II).

Although bursts gradually synchronized throughout the whole area, the burst parameters recovered differently in each channel (Fig. 8b). In contrast, the average profiles of single spikes in each channel were similar to those in previous periods. Thus, Xe molecules apparently have little effect on single spikes even during depressurization. However, when

the synchronized burst rate became large enough, neurons that often fired single spikes under the Xe pressure became calm. Since there are only a few electrodes exhibiting the frequent firing, the change of firing pattern does not affect the overall *SR* value. This indicates that Xe affects not only the bursting spike activity but also the single spike activity.

Period (IV): Recovery of electric activity after gas purge

Even though the system pressure did not change, the purging of the air to completely remove the Xe significantly changed the firing activity. The response to the purge process appeared to have two stages. In the first stage, the synchronized burst rises quickly within the first 10 min (see Figs. 9a and 10(i)). Both *SR* and *SBR* increased simultaneously, mainly due to the further decrease of *IBI*. Other profiles of these bursts (Fig. 10a(i)) resemble those in the depressurization process (Figs. 9b-d). In this stage, relatively few single spikes occurred between bursts. The early stage usually lasted for 15~20 min and each burst parameter gradually approached that of the control period. In the second stage, *SBR* is lower (Fig. 10(ii)). After about one hour, *SBR* approaches 10 counts/min, *IBI* becomes constant at approximately 7 s, *BD* converges to 0.1~0.5 s, and the range of *SIB* settles to 10~ 40 cpb (Figs. 9b-d), all being comparable to their values in the control period.

After period (IV), we monitored the firing activities for several days to verify the health of the treated sample. In a few cases, the firing activity slightly differed from that of the control period at the end of the experiment. However, even in such samples, the firing activity returned to that of the control period within the variation range after we incubated the sample under the physiological environment for a few days. Microscope observations of the cell shape of the neuronal networks after the experiments showed no abnormalities.

DISCUSSION

Inhibition process of firing activity by Xe under pressure

The similarities between the burst profiles and those in the previous study by Chiappalone et al., [2006] indicate that the neuronal networks studied here were sufficiently mature. As such, we conclude that the networks were well-connected by robust intercellular connections and consisted of close circuits. The similarities also suggest that both NMDA and non-NMDA receptor channels were expressed at the excitatory synapses.

After the Xe pressurization, both the cell shape and single-spike profiles remained essentially unchanged. This result indicates that a quadrupling of hydrostatic pressure (to 0.4 MPa) has little effect on the neuronal activity. However, the Xe pressure jump caused a sudden decrease in both *SR* and *SBR* with *SBR* reaching essentially zero approximately 10-min after pressurization, although more than 60% of the electrodes continued to fire. At that moment, the burst profiles (e.g., these in Figs. 7b-d) resembled those observed in the immature network of Kamioka et al. [1996] and Chiappalone et al. [2006]. Given the maturity of the network prior to pressurization, this apparent immature network condition might come from the inhibition of synapse transmission by Xe molecules dissolved in the culture medium.

The results support an obstruction mechanism of general anesthesia but not the lipid solubility hypothesis. The lipid solubility hypothesis requires the inhibition of neuronal firing [Meyer, 1937; Miller et al., 1965; 1969; Lever et al., 1971; Koski et al., 1973; O'leary, 1984], but we observed the neurons to continue firing. Instead, the Xe appears to function via an obstruction mechanism. For example, the dissolved Xe molecules may act as a channel blocker at the synaptic junction [e.g., Franks et al., 1998; Dinse et al., 2005]. Another obstruction mechanism, the hydrate hypothesis, is unlikely because our experimental conditions were not stable conditions for Xe-hydrate crystals. But a modified hydrate hypothesis may work: dissolved Xe molecules may obstruct synapse transmission via the formation of a hydrate-like water structure around the Xe molecules. Such structure was found in a study of the dissolution of the clathrate-forming molecules [Uchida et al., 2003]. Thus dissolved Xe molecules may obstruct the synapse transmission. The obtained

experimental results can be explained by the latter two hypotheses. We conclude that the inhibition of electric activity of neuronal network is mainly caused by the Xe molecules obstructing synapse transmission.

Recovery of electric activity of neuronal network by Xe depressurization

As with the pressurization, the pressure release left the cell shape and the single-spike profiles essentially unchanged. Moreover, we observed no indication of gas bubbles. Thus the neuronal network appears to lose the dissolved Xe molecules very slowly.

The slow loss of Xe molecules agrees with the slow recovery of the synchronized bursts after Xe depressurization. After the bursts appear, *SBR* increases gradually and much more slowly than the rate of decrease during pressurization. Also, the burst profiles differ slightly from those in the control period, resembling instead those in the early stage of neuronal network formation (e.g., Chiappalone et al. [2006]). The results suggest that the recovery of the synchronized burst involves a gradual decrease of Xe concentration in the synaptic junctions. The behavior of the network in the slow-recovery period resembles that of an immature network, despite the network's maturity.

Purging the vapor in the vessel with fresh air (with 5% CO_2) produces a rapid increase of network firing (*SR* and *SBR* in Fig. 9a). This change would be caused by the decrease of Xe concentration in the vapor, which would accelerate the removal of Xe molecules from the medium, and thus from the inhibiting synaptic sites. A sudden re-connection of numerous synapses in the neuronal network would cause the observed frequent bursting, which is characterized by smaller *BD* (but similar *SIB*) and shorter *IBI* just after the purging (Figs. 9b-d). Frequent bursts like this (Fig. 10b(i)) have been seen in previous studies [Chiappalone et al., 2006] when a cultured network becomes mature. Thus, similar conditions of network maturation may have occurred during purging, leading to the rapid bursting.

The profiles and the spike rate of the single spikes did not change significantly over the whole experiment. This is strong evidence that Xe molecules do not affect the firing activity of the neuron itself. Although the non-burst single-spike rate tends to increase slightly while the synchronized bursts are inhibited, the change contributes little to *SR*. This result suggests that the change of the firing activities, such as the burst profiles, is not affected by Xe inhibition but is related to the change of the electric signals from neighboring neurons, that is, the change of the electric circuit in the neuronal network.

After the purge, the firing pattern gradually changed over several tens of minutes, going from the frequent burst stage to one that was similar to that in the control period. Although the firing profiles did not fully recover to the original condition 1-h after purging, the results indicate that the pressurization of Xe gas does not damage the neuronal network physically, yet inhibits the synaptic transmission in the neuronal network temporally and reversibly.

CONCLUSIONS

This study revealed that dissolved Xe molecules reversibly inhibit the firing activity of the neuronal network of cortical culture. As the Xe largely left single spikes unchanged while completely inhibiting synchronized bursts, the Xe molecules acted more as a transmission inhibitor in the neuronal network, not as a firing inhibitor of the neuron itself. The burst profiles gradually recovered after depressurization, later recovering much more rapidly when the Xe was purged from the system. This recovery may be due to an increase in the number of recovered connections in the neuronal network. By comparing to previous work, we argued that the inhibition was caused by a temporal inhibition of the synapse transmission by the dissolved Xe molecules. The results are not consistent with the lipid solubility hypothesis for general anesthesia, but support two other proposed hypotheses: the channel-blocker hypothesis and a modified hydrate hypothesis. Further, molecular-level details of the inhibition process of transmission at synapses should be revealed in the future.

Acknowledgments

This work was partly supported financially by a Grant-in-Aid for Scientific Research from the Japan Society for the Promotion of Science (grant no. 17340125 and 23350001). We thank Dr. Jon Nelson for his proofreading and valuable comments and suggestions which improved the manuscript.

Reference

Banno M, Mizuno T, Kato H, Zhang G, Kawanokuchi J, Wang J, Kuno R, Jin S, Takeuchi H, Suzumura A (2005), The radical scavenger edaravone prevents oxidative neurotoxicity induced by peroxynitrite and activated microglia. Neuropharmacology 48:283-290.

Ben-Ari Y (2001), Developing networks play a similar melody. Trends Neurosci 24:353-360.

Chiappalone M, Bove M, Vato A, Tedesco M, Martinoia S (2006), Dissociated cortical networks show spontaneously correlated activity pattern during in vitro development. Brain Res 1093:41-53.

Corner MA, van Pelt J, Wolters PS, Baker RE, Nuytinck RH (2002), Physiological effects of sustained blockade of excitatory synaptic transmission on spontaneously active developing neuronal networks – an inquiry into the reciprocal linkage between intrinsic biorhythms and neuroplasticity in early ontogeny. Neurosci Biobehav Rev 26:127-185.

Cullen SC, Gross EG (1951), The anesthetic properties of xenon in animals and human beings, with additional observations on krypton, Science 113:580-582.

de Sousa SLM, Dickinson R, Lieb WR, Franks NP (2000), Contrasting synaptic actions of the inhalational general anesthetics isoflurane and xenon. Anesthesiology 92:1055-1066.

Dinse A, Fohr KJ, Georgieff M, Beyer C, Bulling A, Weight HU (2005), Xenon reduces glutamate-, AMPA-, and kainite-induced membrane currents in cortical neurons. British J Anesthesia 94:479-485.

Dorsch RR (1970), Intermolecular forces, gas hydrates and gaseous anesthesia. Ph.D. thesis Faculty of the graduate school of the Univ. Maryland; pp.157.

Dorsch RR, deRocco (1973), A generalized hydrate mechanism for gaseous anesthesia: part I. Theyory Physiol Chem & Physics 5:209-223

Dorsch RR, Distefano V (1973), A generalized hydrate mechanism for gaseous anesthesia: part II. Experimental Physiol Chem & Physics 5:225-236

Franks NP, Lieb WR (1982), Molecular mechanisms of general anesthesia. Nature 300:487-493.

Franks NP, Lieb WR (1988), Volatile general anesthetics activate a novel neuronal K+ current. Nature 333:662-664.

Franks NP, Dickinson R, de Sousa SLM, Hall AC, Lieb WR (1998), How does xenon produce anaesthesia? Nature 396:324

Franks NP, Lieb WR (1994), Molecular and cellular mechanisms of general anesthesia. Nature 367: 607-614

Georgiev SK, Furue H, Baba H, Kohno T (2010), Xenon inhibits excitatory but not inhibitory transmission in rat spinal cord dorsal horn neurons. Molecular Pain 6:25.

Goto T, Saito H, Nakata Y, Uezono S, Ichinose F, Morita S (1997), Emergence times from xenon anaesthesia are independent of the duration of anaesthesia. Br. J. Anaesth.79:595-599.

Gross GW (1979), Simultaneous single unit recording in vitro with a photoetched laser deinsulated gold multielectrode surface. IEEE Trans Biomed Eng 26:273-279.

Gross GW, Schwalm, FU (1994), A closed flow chamber for long-term multichannel recording and optical monitoring. J Neurosci Meth 52:73-85.

Haseneder R, Kratzer S, Kochs E, Eckle V-S, Zieglgansberger W, Rammes G (2008), Xenon Reduces N-Methyl-D-aspartate and-Amino-3-hydroxy-5-methyl-4-isoxazolepropionic Acid Receptor–mediated Synaptic Transmission in the Amygdala. Anesthesiology 109:998-1006.

Honma S, Shirakawa T, Katsuno Y, Namihira M, Honma K (1998), Circadian periods of single suprachiasmatic neurons in rats. Neurosci Lett 250:157-160.

Hosokawa C, Kudoh SN, Kiyohara A, Taguchi T (2008), Resynchronization in neuronal network divided

by femtosecond laser processing. NeuroReport 19:771-775.

Ito D, Tamate H, Nagayama M, Uchida T, Kudoh SN, Gohara K (2010), Minimum neuron density for synchronized bursts in a rat cortical culture on multi-electrode arrays. Neuroscience 171:50-61.

Jimbo Y, Tateno T, Robinson HPC (1999), Simultaneous induction of pathway-specific potentiation and depression in networks of cortical neurons. Biophys J 76:670-678.

Kamioka H, Maeda E, Jimbo Y, Robinson HPC, Kawana A (1996), Spontaneous periodic synchronized bursting during formation of mature patterns of connections in cortical cultures. Neurosci Lett 206:109-112.

Khazipov R, Sirota A, Leinekugel X, Holmes GL, Ben-Ari Y, Buzsaki G (2004), Early motor activity drives spindle bursts in the developing somatosensory cortex. Nature 432:758-761.

Koski WS, Kaufman JJ, Wilson KM (1973), Physicochemical aspects of the action of general anesthetics. Nature 242:65-66.

Kudoh SN, Hosokawa C, Kiyohara A, Taguchi T, Hayashi I (2007), Biomodeling system - interaction between living neuronal networks and the other world. J Robot Mech 19:592-600.

Lever MJ, Miller KW, Paton WDM, Smith EB (1971), Pressure reversal of anesthesia. Nature 231:368-371.

Ma D, Wilhelm S, Maze M, Franks NP (2002), Neuroprotective and neurotoxic properties of the 'inert' gas, xenon. British J Anesthesia 89:739-746.

Matsumoto J (1995), Molecular mechanism of biological responses to homoeopathic medicines. Medical Hypotheses 45:292-296.

Mayer KH (1937), Contributions to the theory of narcosis. Trans Faraday Soc 33:1062-1069.

Mihic SJ, Ye Q, Wick MJ, Koltchine VV, Krasowski MD, Finn SE, Mascia MP, Valenzuela CF, Hanson KK, Greenblatt EP, Harris RA, Harrison NL (1997), Sites of alcohol and volatile anaesthetic action on $GABA_A$ and glycine receptors. Nature 389:385-389.

Miller SL (1961), A theory of gaseous anesthethics. Proc Nat Acad Sci 47:1515-1524.

Miller KW, Paton WDM, Smith EB (1965), Site of action of general anaesthetics. Nature 206:574-577

Miller KW (1969), How do anesthetics work?, Anesthesiology 30:127-128.

Mizuno T, Kurotani T, Komatsu Y, Kawanouchi J, Kato H, Mitsuma N, Suzumura A (2004), Neuroprotective role of phosphodiesterase inhibitor ibudilast on neuronal cell death induced by activated microglia. europharmacology 46:404-411.

Mukai Y, Shiina T, Jimbo Y (2003), Continuous monitoring of developmental activity changes in cultured cortical networks. Electr Eng Jpn 145:28-37.

Negale P, Metz LB, Crowder CM (2005), Xenon acts by inhibition of non-N-methyl-D-aspartate receptor – mediated glutamatergic neurotransmission in caenrhabditis elegans. Anesthesiology 103:508-513.

O'leary T (1984), A model for the interaction of anesthetics with the phospholipids membrane headgroup-interface region. Biochim Biophys Acta 769:197-200.

Opitz T, De Lima AD, Voigt T (2002), Spontaneous development of synchronous oscillatory activity during maturation of cortical networks in vitro. J Neurophysiol 88:2196-2206.

Pauling L (1961), A molecular theory of general anesthesia. Science 134:15-21.

Pine J (1980), Recording action potentials from cultured neurons with extracellular microcircuit electrodes. J Neurosci Methods 2:19-31.

Plested AJR, Wildman SS, Lieb WR, Franks NP (2004), Determinants of the sensitivity of AMPA receptors to xenon. Anesthesiology 100:347-358.

Preckel B, Weber, NC, Sanders, RD, Maze, M, Schlack W (2006), Molecular mechanisms transducing the anesthetic, analgesic, and orga-protective actions of xenon. Anesthesiology 205:187-197.

Robinson HP, Kawahara M, Jimbo Y, Torimitsu K, Kuroda Y, Kawana A (1993), Periodic synchronized bursting and intracellular calcium transients elicited by low magnesium in cultured cortical neurons. J Neurophysiol 70:1606-1616.

Schoenborn BP, Featherstone RM, Vogelhut PO, Susskind C (1964), Influence of xenon on protein hydration as measured by a microwave absorption technique. Nature 202:695-696.

Takeuchi H, Mizuno T, Zhang G, Wang J, Kawanokuchi J, Kuno R, Suzumura A (2005), Neuritic beading

induced by activated microglia is an early feature of neuronal dysfunction toward neuronal death by inhibition of mitochondrial respiration and axonal transport. J Biol Chem 280:10444-10454.

Uchida T, Ohmura R, Nagao J, Takeya S, Ebinuma T, Narita H (2003), Viscosity of aqueous CO_2 solutions measured by dynamic light scattering. J. Chem. Eng. Data 48:1225-1229.

van Pelt J, Wolters PS, Corner MA, Rutten WLC, Ramarkers GJA (2004), Long-term characterization of firing dynamics of spontaneous bursts in cultured neural networks. IEEE Trans Biomed Eng 51:2051-2062.

Wagenaar DA, Pine J, Potter SM (2006), An extremely rich repertoire of bursting patterns during the development of cortical cultures. BMC Neurosci 7:11.

Figure captions

Fig. 1: The experimental system. The cortical neuronal network grown on a multi-electrode array (MEA) is set in the MED connector within a high-pressure vessel in the incubator.

Fig. 2: Typical traces of pressure (left scale) and temperature (right scale) during one experimental run. (I) control period, (II) pressurizing period, (III) pressure-release period, (IV) purge period

Fig. 3: Profile parameters for (a) single spikes and (b) bursts. Typical quantity of each parameter in the control period is also shown.

Fig. 4: Sample used and data from the control (I) period. (a) Photomicrographs of the cortical cells on (left) 1 day in vitro (DIV) and (right) 20 DIV (the experimental day). The black squares are the 50×50 μm^2 electrodes (center-center spacing of 150 μm). Isolated cells are observed clearly at 1 DIV, and they grew until a confluent mono-layer formed by 20 DIV. (b) Total spike rate of 16 electrodes (*SR*) for 25days cultivation. Neurons start firing at about one week and *SR* increases until *SR* reaches to the saturation value at about two weeks. After about 15 DIV, *SR* becomes constant with relatively large scattering.

Fig. 5: Typical firing activity data in the control (I) period for the sample at 20 DIV. (a) Snapshot of typical synchronized burst signals measured on MEA. A synchronized burst is recorded at all electrodes although the burst profiles vary in each electrode. The number of each signal block is the channel number corresponding to each electrode. The skipped channel numbers provide space in the spike raster plot. (b) The spike raster plot. Channel number corresponds to each electrode that appears in (a). Most bursts are synchronized in every electrode.

Fig. 6: Firing activity in the pressurizing (II) period for the sample at 20 DIV. (a) 5 min, (b) 10 min, and (c) 15 min after the 0.3-MPa Xe pressurization. The synchronized bursts disappeared after 10 min, but the single spikes remain. (d) The spike raster plot at 15 min. Most signals are the single spikes. No synchronized firings are observed during this period.

Fig. 7: Change in firing activity profiles from the control (I) to the pressurization (II) periods. At 6 min, 0.3 MPa Xe gas was applied. (a) Spike rate (*SR*; solid diamonds, left scale), non-burst single spike rate (solid circles, left scale) and synchronized burst rate (*SBR*; open triangles, right scale). All three are the total value of all 16 electrodes and are averaged every 5 min. Time series of three burst parameters observed on a typical channel: (b) Burst duration (*BD*). (c) Inter-burst interval (*IBI*). (d) Number of spikes per burst (*SIB*). No significant changes are observed in all three parameters. Until 4 min after Xe pressurization, burst signals are completely absent. The sudden decrease of *SR* after pressurization results from the disappearance of synchronized bursts. The non-burst single-spike rate does not change remarkably.

Fig. 8: Firing activity in the pressure-release (III) period for the sample at 20 DIV. (a) Snapshot of the MEA signals on the MED probe. The synchronized bursts begin to appear. (b) Spike raster plot 10-min into period III. The synchronized bursts are recorded on several firing electrodes but not on all electrodes.

Fig. 9: Change in firing activity profiles from the pressure-release (III) to the purge (IV) periods. (a) Spike rate (*SR*; solid diamond, left scale), non-burst single spike rate (solid circles, left scale) and synchronized burst rate (*SBR*; open triangle, right scale). All three are the total value of all 16 electrodes and are averaged every 5 min. Time series of three burst profiles observed on a typical channel: (b) Burst duration (*BD*). (c) Inter-burst interval (*IBI*). Inset shows enlarged scale for period IV. (d) Number of spikes per burst (*SIB*). As *SBR* increases in period (III), *IBI* comes down from infinity to several tens of seconds. *SIB* also increases

gradually with an increase in *SBR*. The *BD* values scatter between 0.1 and 1 s. Just after purging the gas in the vessel, *SR* and *SBR* temporally increase, which is caused by the appearance of frequent bursts. When both *SR* and *SBR* reach to relatively constant values at about 30 min after purging, three burst parameters also become constant.

Fig. 10: Firing activity in the purge (IV) period for the sample at 20 DIV. (a) Snapshots of the MEA signals on the MED probe. (b) Spike raster plots. Upper (i) shows the rapid bursting condition and begins 4-min after the purge; lower (ii) shows the firing conditions near the end of the experimental period and begins 24-min after the purge.

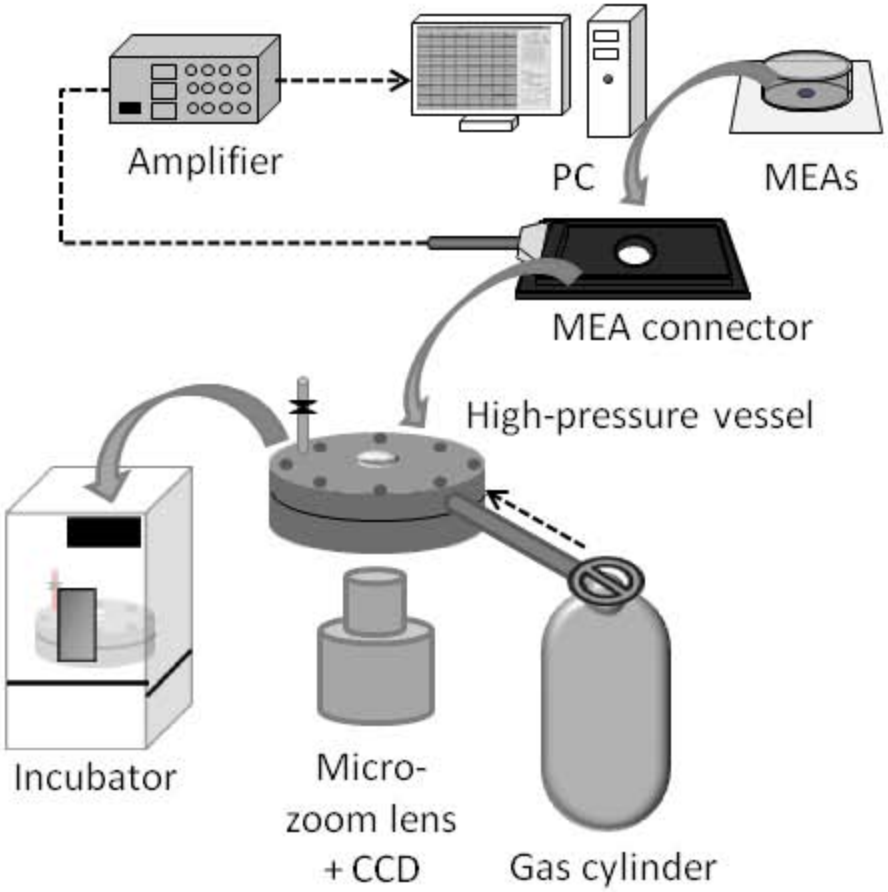
Amplifier
PC
MEAs
MEA connector
High-pressure vessel
Incubator
Micro-
zoom lens
+ CCD
Gas cylinder

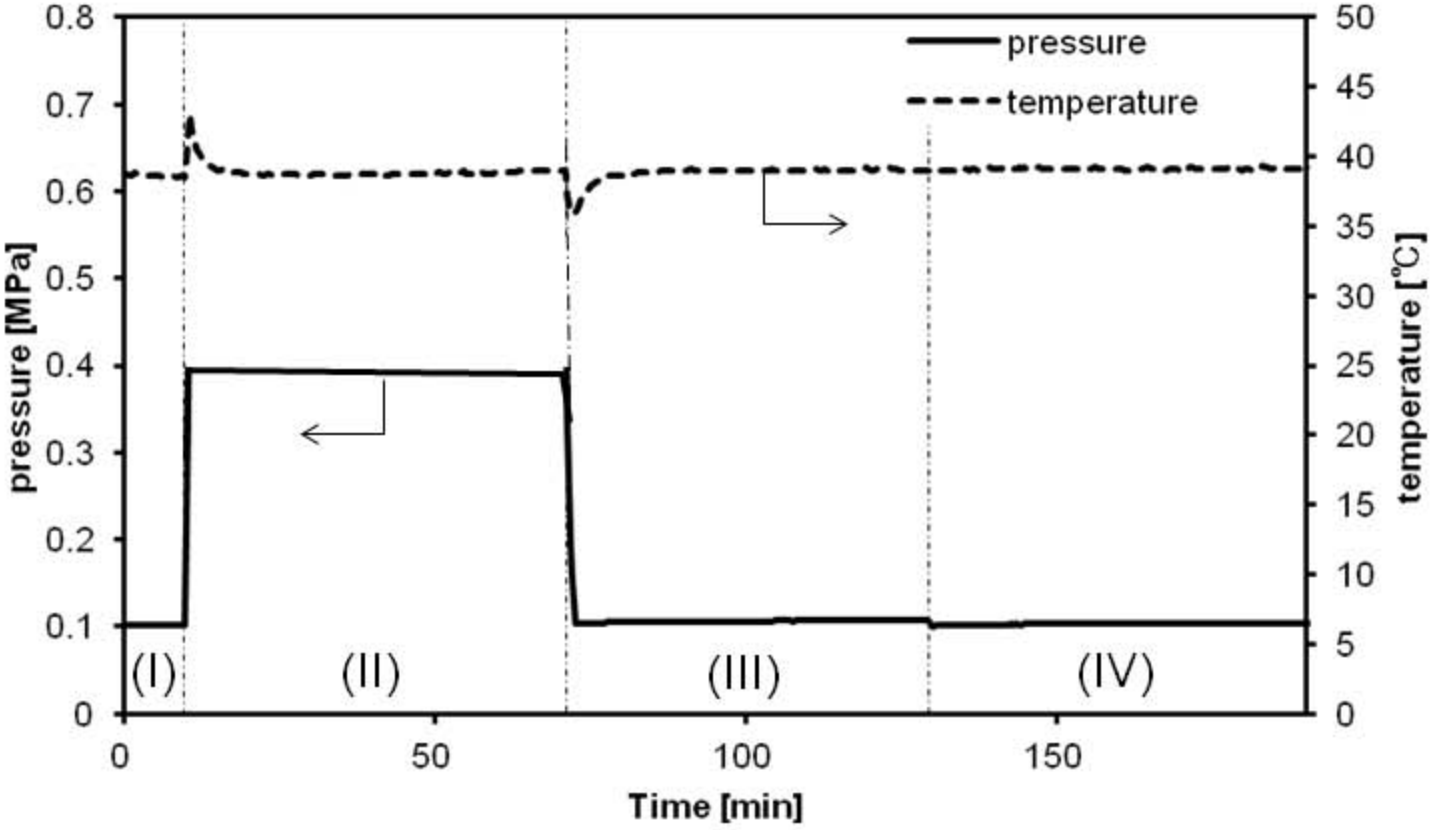
pressure
temperature
pressure [MPa]
temperature [°C]
Time [min]
(I)
(II)
(III)
(IV)
0
0.1
0.2
0.3
0.4
0.5
0.6
0.7
0.8
0
5
10
15
20
25
30
35
40
45
50
0
50
100
150

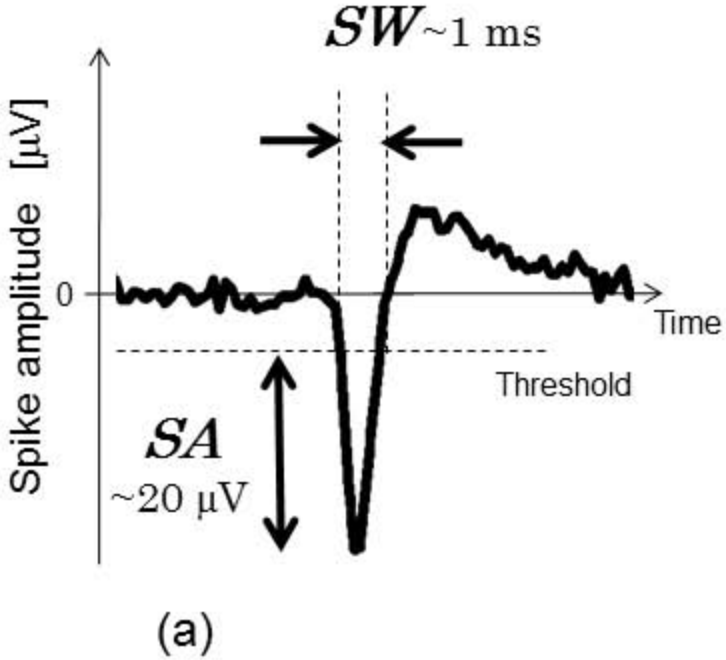
SW~1 ms
Spike amplitude [μV]
0
Time
Threshold
SA
~20 μV

(a)

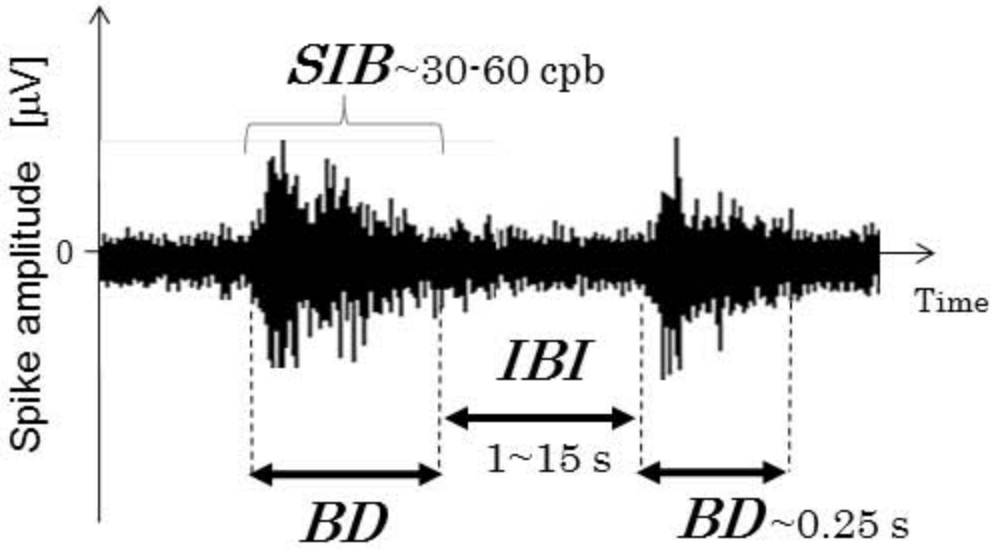
SIB~30-60 cpb
Spike amplitude [μV]
0
Time
IBI
1~15 s
BD
BD~0.25 s

(b)

(a)

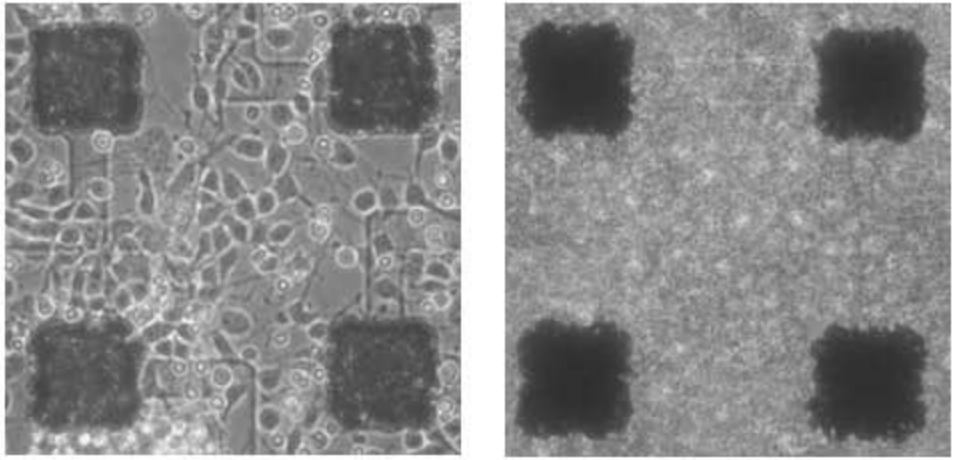

(b)

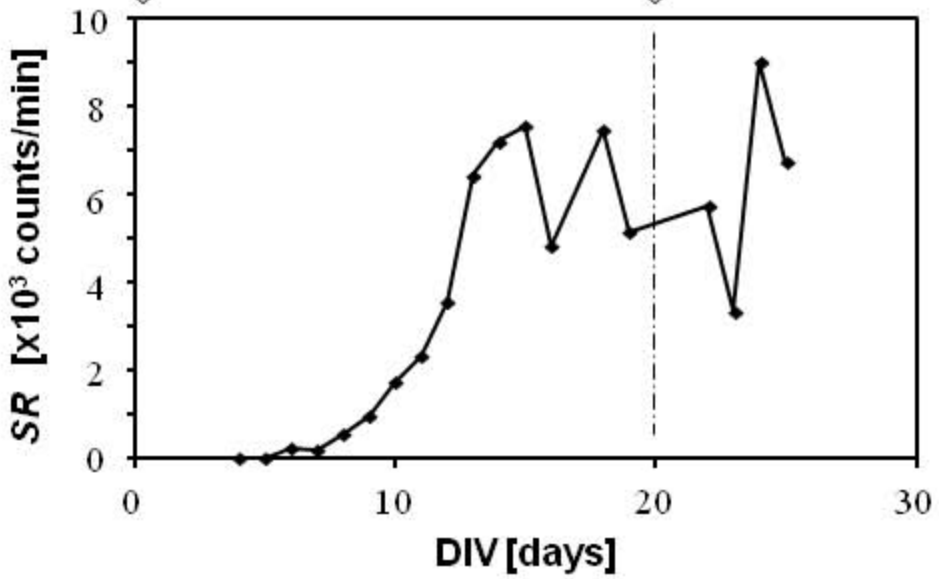

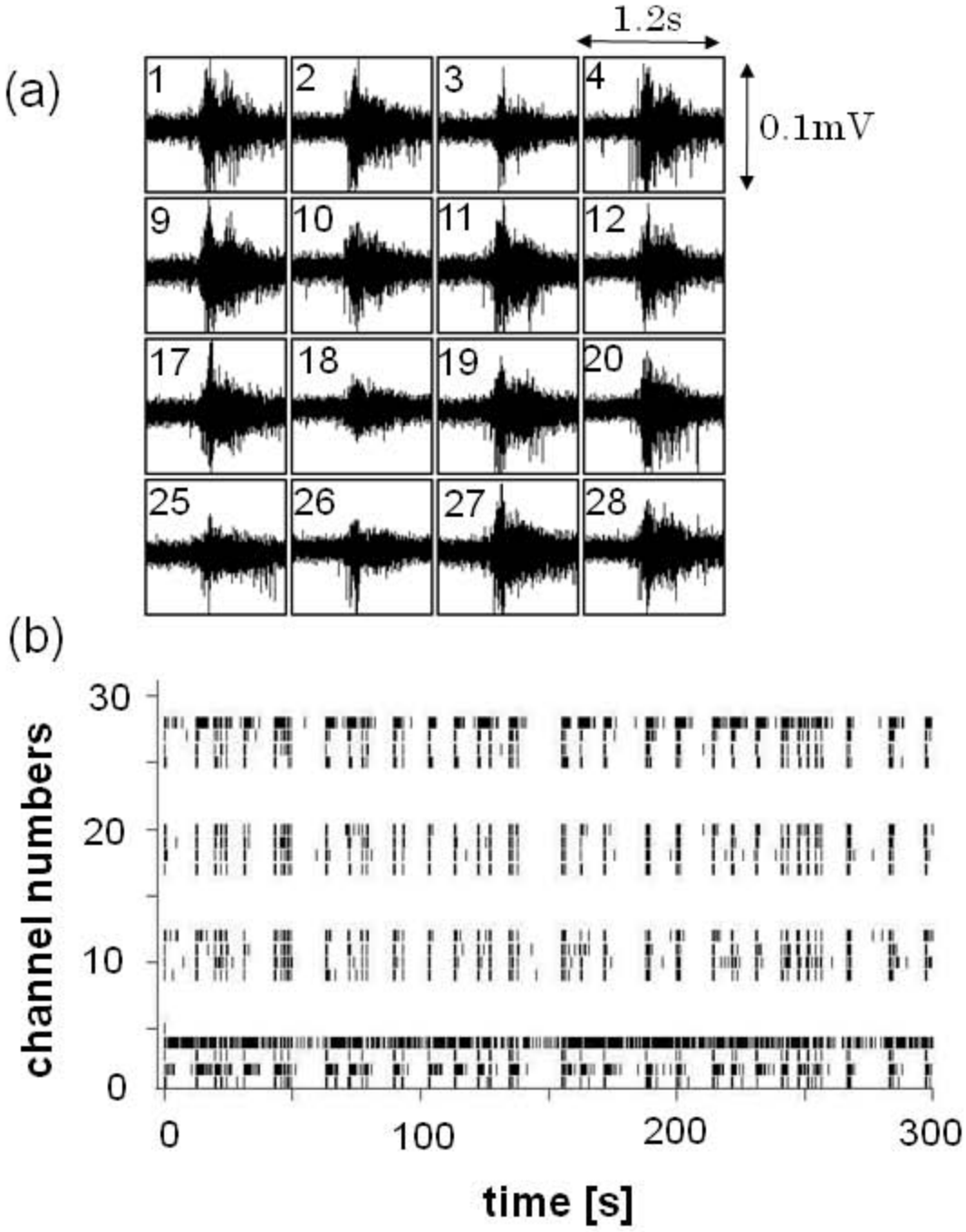
(a)
1.2s
0.1mV
1
2
3
4
9
10
11
12
17
18
19
20
25
26
27
28
(b)
channel numbers
30
20
10
0
0
100
200
300
time [s]

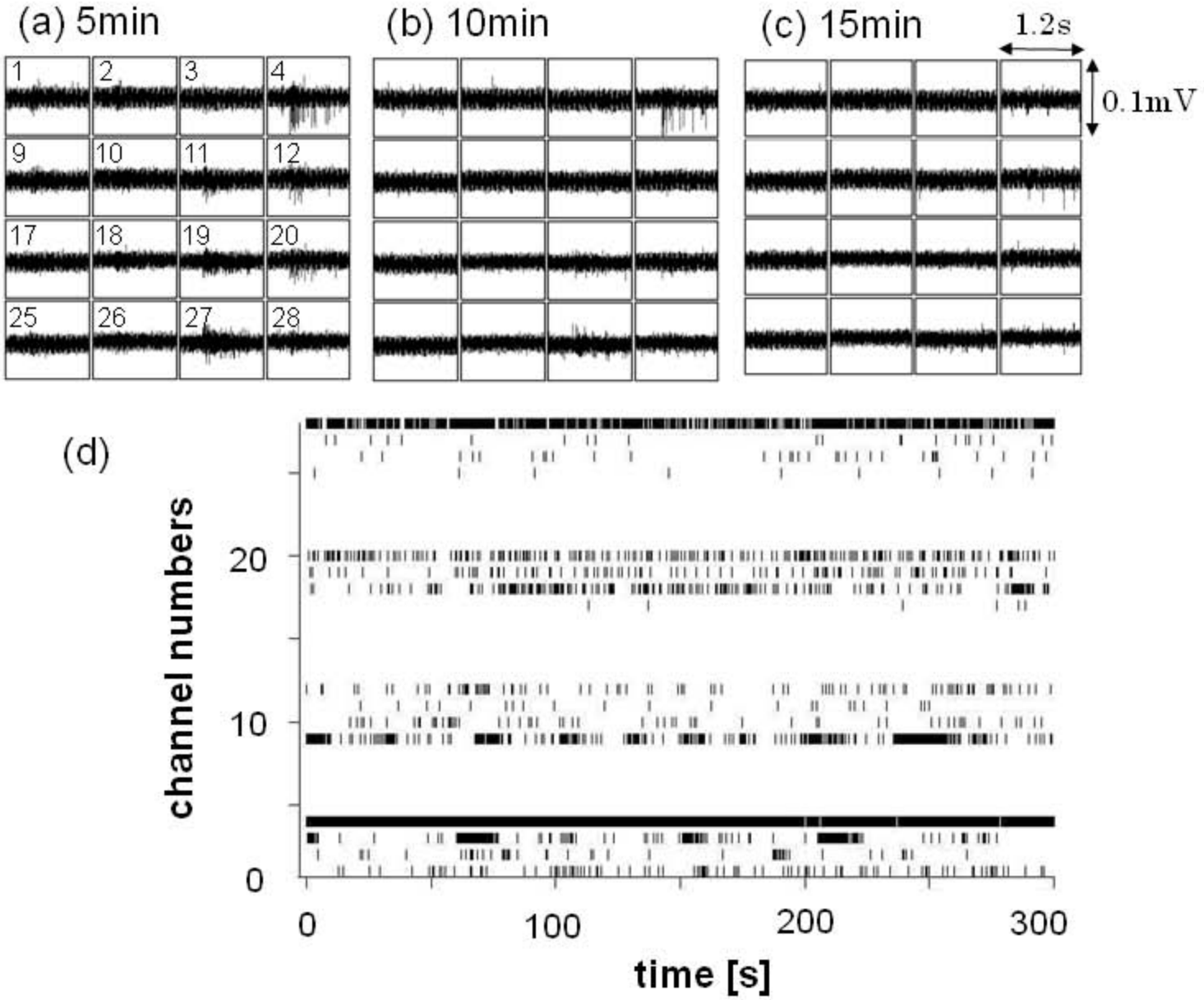
(a) 5min
(b) 10min
(c) 15min
1.2s
0.1mV
1
2
3
4
9
10
11
12
17
18
19
20
25
26
27
28
(d)
channel numbers
0
10
20
0
100
200
300
time [s]

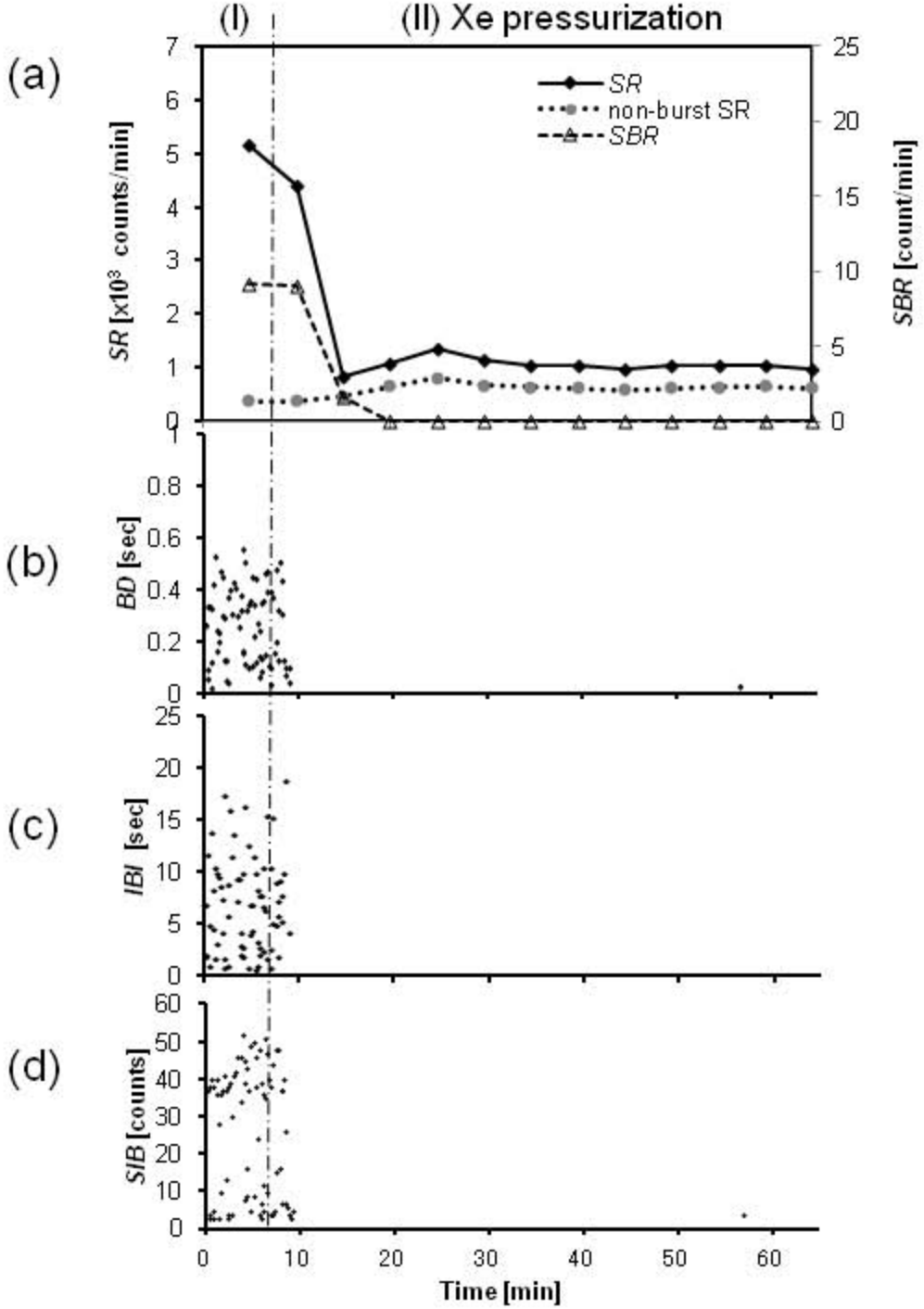
(I)
(II) Xe pressurization
(a)
(b)
(c)
(d)
SR
non-burst SR
SBR
SR [x10³ counts/min]
SBR [count/min]
BD [sec]
IBI [sec]
SIB [counts]
Time [min]

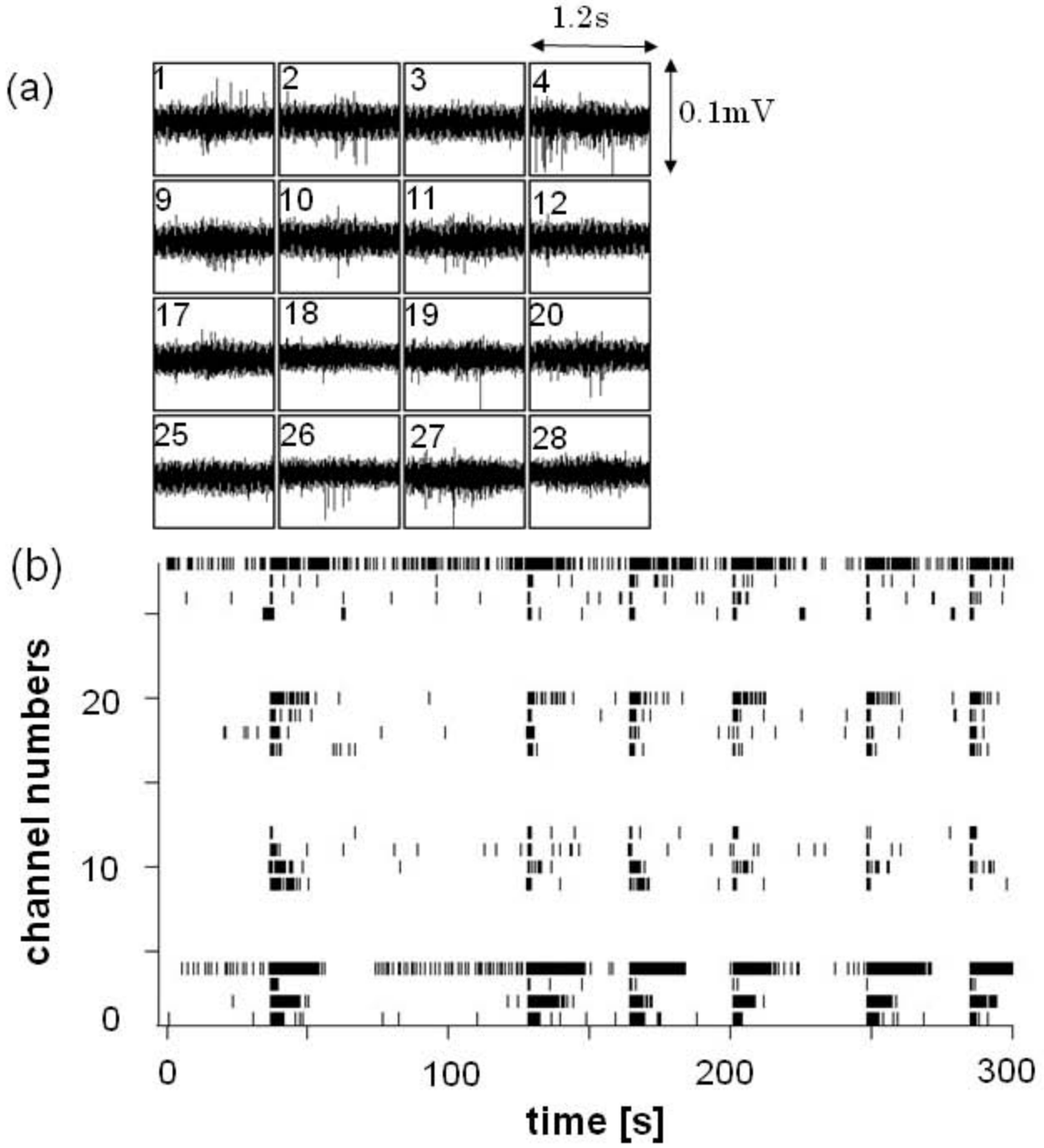
(a)
1.2s
0.1mV
1
2
3
4
9
10
11
12
17
18
19
20
25
26
27
28
(b)
channel numbers
0
10
20
0
100
200
300
time [s]

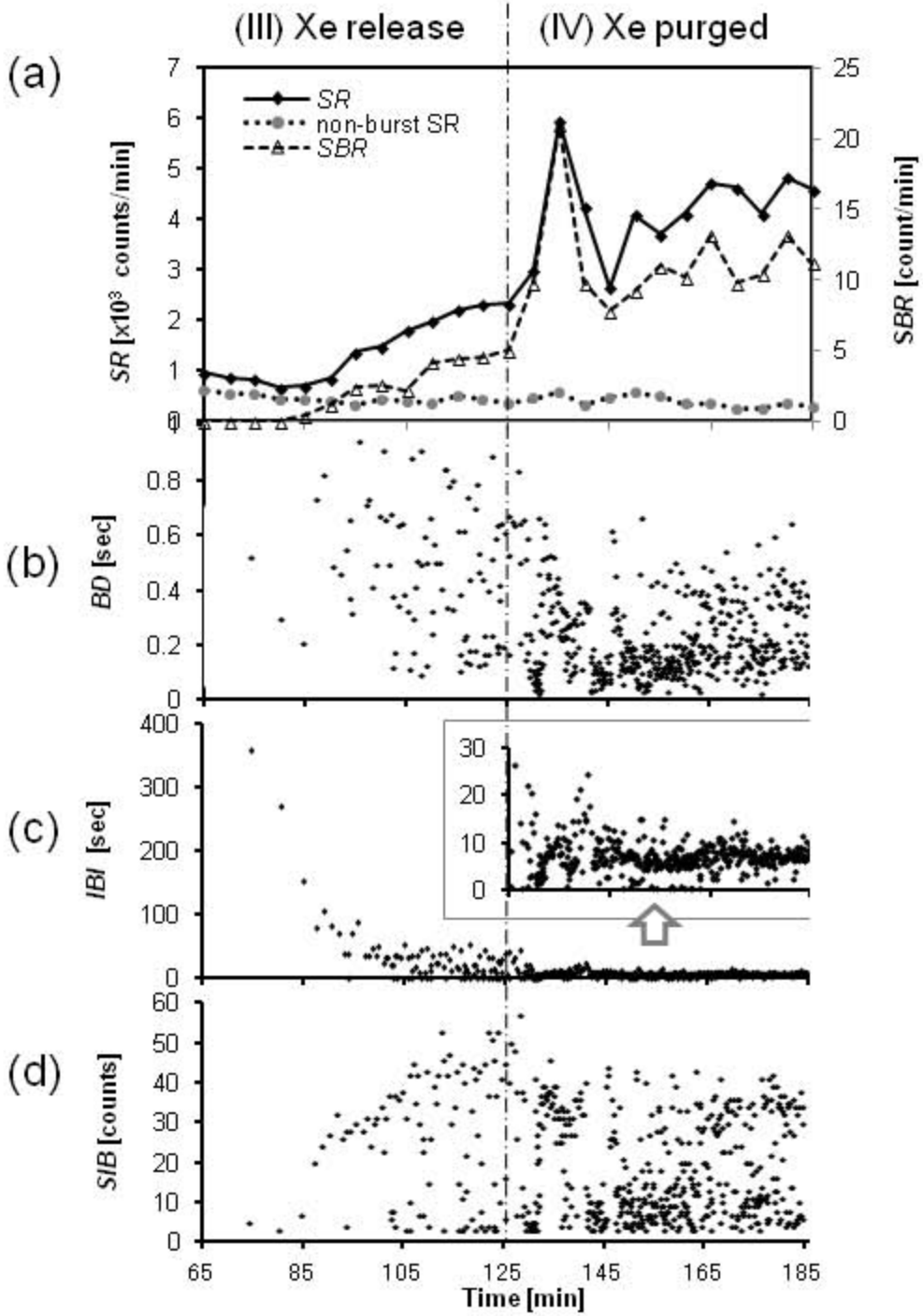
(III) Xe release
(IV) Xe purged
(a)
SR
non-burst SR
SBR
SR [x10³ counts/min]
SBR [count/min]
(b)
BD [sec]
(c)
IBI [sec]
(d)
SIB [counts]
Time [min]

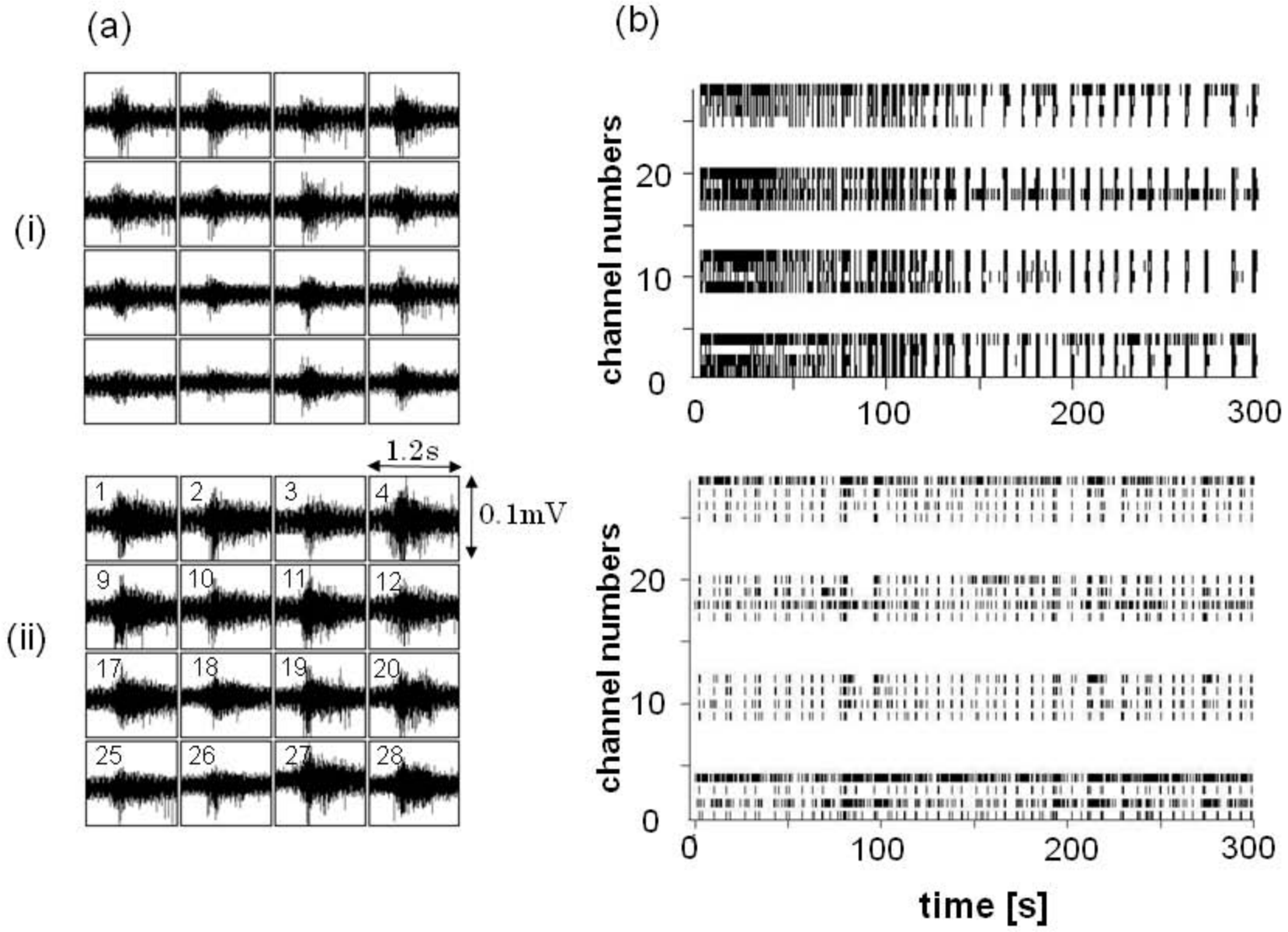
(a)
(i)
(ii)
1.2s
0.1mV
1
2
3
4
9
10
11
12
17
18
19
20
25
26
27
28
(b)
channel numbers
0
10
20
0
100
200
300
channel numbers
0
10
20
0
100
200
300
time [s]